ON-LINE IDENTIFICATION OF HYDRODYNAMICS IN UNDERWATER VEHICLES

Mario A. Jordán [*,1], **Jorge L. Bustamante** [*], **Edwin Kreuzer** [**] and **Volker Schlegel** [**]

[*] *Department of Electrical Engineering and Computers, Universidad Nacional del Sur Av. Alem 1253, 8000 Bahía Blanca, Argentina*
[**] *Mechanics and Ocean Engineering, Technical University Hamburg-Harburg Eissendorfer Strasse 42, D-21073 Hamburg, Germany*

Abstract: In this work an algorithm for on-line estimation of the nonlinear hydrodynamics in underwater vehicles is presented. The algorithm is able to estimate physical parameters from natural operation signals. Identifiability and convergence of the parameter trajectories are analyzed. The application of the algorithm to a spherical vehicle is described with numerical simulations.

Keywords: Nonlinear Hydrodynamics - Underwater Vehicles - On-line Identification - Persistency of Excitation

1. INTRODUCTION

Remotely operated vehicles (ROVs) play an important role in the offshore industry. The use of conventional control systems for ROVs is limited in that the hydrodynamic coefficients of a particular vehicle are not usually known until after the vehicle has been completely design and test facilities, such as a wind tunnel or a wave tank, are employed for their determination. For dynamical positioning it is required the tracking and positioning of the vehicle to precisions ranging a few centimeters with short settling times.

Usually the model of the dynamics contains important structural uncertainties in the nonlinear characteristics of the frictional and pressure drag forces. These uncertainties makes difficult to achieve good behaviors and commonly the application of robust control can ensure stability at the cost of performance degradation (Caccia and Veruggio, 2000; Do *et al.*, 2004).

Due to the usual open frame architecture of ROVs, complex forms in the geometry ranging from a spherical, prismatic, prolate ellipsoid forms, the determination of hydrodynamics characteristics in the design phase and in posterior modifications is very complex.

The application of identification techniques with real signals of the kinematic and dynamics during ROV operation can provide a good method for uncertainty reduction. The on-line parameter identification has proven to be a general means to achieve adaptation to unknown modifications of physical parameters of the dynamics and its environment (Beltrán and Jordán, 2004). These strategies of parameter estimation provide a first link in the design of adaptive controllers and constitutes an alternative to expensive experimentation with scale models in test facilities.

In this work a method for adaptive on-line estimation is presented for the identification of pressure drag characteristics and added mass of a ROV. The algorithm is applicable for general geometric shapes of the ROV and can be used for self-

[1] Corresponding author: Mario Alberto Jordán: e-mail: mjordan@criba.edu.ar; phone +54 291 4595100 (3310)

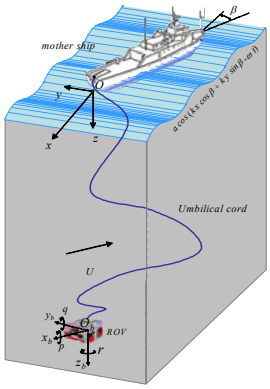

Fig. 1. Earth- and body-fixed frames for ROV motion characterization

tuning of model coefficients which are previously unknown. A case study for a sphere shaped ROV illustrates by means of numerical simulations the feature of the algorithm under simple motions.

2. ROV DYNAMICS

A mathematical nonlinear model for a ROV having three planes of symmetry and moving with 6 degrees of freedom can be described in a body-fixed frame as (see Fig. (1) and cf. Fossen, 1994, for conventions)

$$M\dot{\mathbf{v}} = -C(\mathbf{v})\mathbf{v} - D(\mathbf{v})\mathbf{v} + \\ +\mathbf{F}_b(\boldsymbol{\eta}) + \mathbf{F}_c + \mathbf{F}_e + \boldsymbol{\tau} \quad (1)$$

$$\dot{\boldsymbol{\eta}} = J(\boldsymbol{\eta})\mathbf{v}, \quad (2)$$

with the matrices

$$M = M_{rov} + M_a \quad (3)$$

$$C(\mathbf{v}) = C_{rov}(\mathbf{v}) + C_a(\mathbf{v}) \quad (4)$$

$$D(\mathbf{v}) = D_0 + D_1(\mathbf{v}), \quad (5)$$

where the generalized position in the earth-fixed frame is denoted by $\boldsymbol{\eta} = [x, y, z, \phi, \theta, \psi]^T$, the vector $\mathbf{v} = [u, v, w, p, q, r]^T$ indicates the generalized velocity vector of the ROV in its flight path in the body-fixed frame, J is a transformation matrix involving the Euler angles roll (ϕ), pitch (θ) and yaw (ψ), M is the inertia matrix composed by the ROV inertia matrix M_{rov} and the added mass matrix M_a, C is the centripetal and Coriolis matrix with a first component C_{rov} for the ROV and a second component for the hydrodynamics C_a, D is the damping matrix composed by a constant matrix D_0 and a velocity depending matrix D_1, $\mathbf{F}_b$ is the net buoyancy force, $\mathbf{F}_c$ the cable reaction force, $\mathbf{F}_e$ environmental forces like currents, and $\boldsymbol{\tau}$ the generalized impulse force of the thrusters.

3. ROV HYDRODYNAMICS

In general, the damping of an underwater vehicle moving in 6 degrees of freedom at high speed is highly nonlinear and strongly coupled. Usually, rough approximations are made based on the assumption that the vehicle moves slowly. The violation of this assumption, specially when high-gain controllers are applied, creates one of the major uncertainty in the dynamics. In this work we investigate the hydrodynamic damping in dependence on the geometric form and usual range of velocities of a ROV in the operation.

A body moving through a fluid experiences a drag force, which is of frictional and of pressure nature. Particularly, the last force is associated with the development of a wake behind a passing flow.

For usual ROV geometries, the pressure drag dominates over frictional drag since their shapes act as bluff bodies offering higher resistance to motion than streamlined bodies. The drag force experimented by body in relative motion with respect to the fluid depends on the Reynolds number defined as

$$\mathrm{Re} = \frac{\rho_{_{H_2O}} d}{\eta_{_{H_2O}}} |v_r| , \quad (6)$$

where v_r is the velocity of the body with respect to moving fluid particles, d the characteristic dimension of the body perpendicular to the direction of v_r, $\rho_{_{H_2O}}$ the salt water density ($\rho = 1026\ [kg/m^3]$) and $\eta_{_{H_2O}}$ the dynamic viscosity of the sea water ($\eta_{_{H_2O}} = 10^{-3}\ [\mathrm{Ns^2/m^2}]$, at $20[^oC]$ and 1 $[atm]$, $\eta_{_{H_2O}} = 1.52 \times 10^{-3}\ [\mathrm{Ns^2/m^2}]$, at $5[^oC]$ and 1 $[atm]$, salinity 3,5%).

A common accepted expression for the drag force is given in (5) (Faltinsen, 1990), where $D(\mathbf{v})$ is a real, skew symmetrical and positive definite matrix with components D_0 being a constant matrix accounting for linear skin friction, and D_1 being a function matrix accounting for quadratic skin friction due to turbulent boundary layer and for damping due to vortex shedding. Thus

$$D_1(\mathbf{v}) = \begin{bmatrix} d_{uu}\,|u| & \cdots & d_{ur}\,|r| \\ \vdots & \ddots & \vdots \\ d_{ru}\,|u| & \cdots & d_{rr}\,|r| \end{bmatrix}, \quad (7)$$

with d_{ij} constant coefficients.

A more accurate approach of these dampings is given in the next. In Fig. (2) the drag coefficient for different shapes is shown. With exception of frontal flat plates, it is seen that C_D is not predictable over a large range in Reynolds number.

Large Reynolds numbers may be usual in the operation of ROVs. This is shown by a simple example. Let a spheric ROV with diameter $d = 1[m]$ have a frontal velocity u varying between 0 till $1[m/s]$, it results a range in Reynolds number from 0 till 10^6 (at 20 $[^oC]$ and 1 $[atm]$). In this range the value of C_D varies significantly in magnitude, particularly about the value $\mathrm{Re} = 10^6$. At a Reynolds number between 10^5 and 10^6, the drag coefficient takes generally a sudden dip (Hideshi, 1989). In particular, near the shoulder, the pressure gradient changes from being nega-

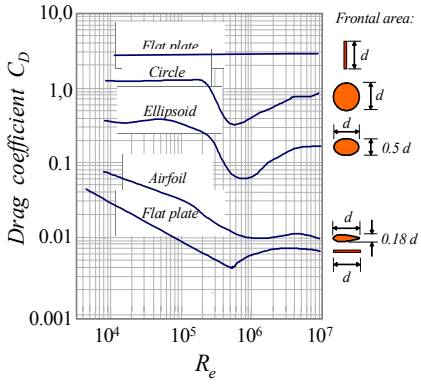

Fig. 2. Drag coefficients for streamlined and bluff bodies

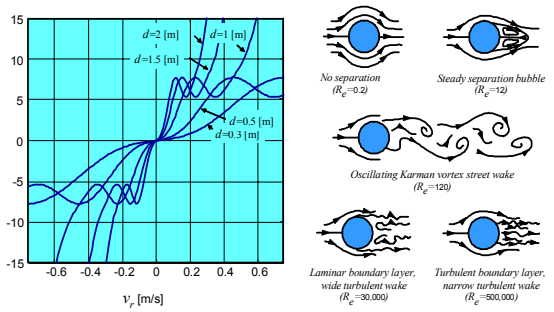

Fig. 3. Drag force and flow patterns for cilindrical body

tive (decreasing pressure) to positive (increasing pressure). The force due to pressure differences changes sign from being an accelerating force to being a retarding force. The curves in Fig. (2) are valid for polished surfaces. When the surface contains certain degree of roughness, then the dips of C_D occur at smaller Reynolds numbers than in the case of the figure (Faltinsen, 1990).

The resulting drag force curves for spherical bodies with different diameters are given in Fig. (3, right). It is worth noticing the functions are not convex in the usual range of that velocity. The development of particular flow patterns with increasing Re accounts for transitions between laminar and turbulent boundary layers as seen in Fig. (3, left). It follows that, if the boundary layer of a sphere can be made turbulent at a lower Reynolds number, then the drag should also go down at that Reynolds number.

In order to capture these hydrodynamics phenomena in the model structure, the following description is used

$$D(\mathbf{v}) = D_0 + D_1(\mathbf{v}) = \tag{8}$$

$$= \begin{bmatrix} \bar{d}_{uu} & \cdots & \bar{d}_{ur} \\ \vdots & \ddots & \vdots \\ \bar{d}_{ru} & \cdots & \bar{d}_{rr} \end{bmatrix} + \tag{9}$$

$$+ \begin{bmatrix} d_{uu}(u) & \cdots & d_{ur}(u,r) \\ \vdots & \ddots & \vdots \\ d_{ru}(r,u) & \cdots & d_{rr}(r) \end{bmatrix}, \tag{10}$$

where $i,j = u,v,...,r$, $\bar{d}_{ij}$ are constants, and $d_{ii}(i)$ and $d_{ij}(i,j)$ are continuous functions in the variables i and j. For instance, for p even

$$d_{ii}(i) = \delta_{ii_1}|i| + \delta_{ii_2}i^2 + \delta_{ii_3}|i|i^2 + \\ + ... + \delta_{ii_{N_0}}i^p \tag{11}$$

$$d_{ij}(i,j) = \delta_{ij_1}|i||j| + \delta_{ij_2}i^2|j| + \delta_{ij_3}|i|j^2 + \\ + \delta_{ij_4}|i|j^3 + \delta_{ij_5}i^3|j| + \delta_{ij_6}i^2j^2 + \\ + ... + \delta_{ij_{N_1}}i^{\frac{p}{2}}j^{\frac{p}{2}}, \tag{12}$$

with δ_{ii_k} and δ_{ij_k} unknown coefficients to be identified, where $N_0 = p$ and $N_1 = \frac{3(p-1)+(p-1)^2}{2}$. It is noticing that the diagonal coefficients d_{ii_k} are described by symmetric functions. Besides, since $D(\mathbf{v})$ is skew symmetric, the non-diagonal elements fulfill $d_{ij}(i,j) = -d_{ji}(j,i)$ for $i \neq j$ in (10). The same occur in (9).

Finally, the hydrodynamics is completed with the hydrodynamic Coriolis and centripetal matrix $C_a(\mathbf{v})$ in (4), which takes the following form for vehicles having 3 planes of symmetry (Fossen, 1994)

$$C_a(\mathbf{v}) = \tag{13}$$

$$\begin{bmatrix} 0 & 0 & 0 & 0 & -c_{\dot{w}}w & c_{\dot{v}}v \\ 0 & 0 & 0 & c_{\dot{w}}w & 0 & -c_{\dot{u}}u \\ 0 & 0 & 0 & -c_{\dot{v}}v & c_{\dot{u}}u & 0 \\ 0 & -c_{\dot{w}}w & c_{\dot{v}}v & 0 & -c_{\dot{r}}r & c_{\dot{q}}q \\ c_{\dot{w}}w & 0 & -c_{\dot{u}}u & c_{\dot{r}}r & 0 & -c_{\dot{p}}p \\ -c_{\dot{v}}v & c_{\dot{u}}u & 0 & -c_{\dot{q}}q & c_{\dot{p}}p & 0 \end{bmatrix}.$$

4. IDENTIFICATION

The goal of the identification consists in estimating the d_{ii_k}'s and d_{ij_k}'s together with the mass and added mass matrix upon measures of the velocity vector $\mathbf{v}$ and the umbilical force $\mathbf{F}_c$ of the ROV system when $\mathbf{F}_e$ is insignificant. A potential numerical problem in the estimation may arrive when the velocity components i,j take values far away from the value 1, namely over or below 1, since the monomials in (11)-(12) will assume values with different order of magnitudes. For this reason it is reasonable to describe (11) and (12) as N piecewise functions of lower order (for instance $p = 4$), defined on N disconnected domains for i and j. For a velocity space decomposed into partitions of N intervals in each dimension, it results

$$\bar{d}_{ii} + d_{ii}(i) = \tag{14}$$

$$\begin{cases} \bar{d}_{ii} + \delta_{ii_{1_1}}|i| + ... + \delta_{ii_{4_1}}i^4, \text{ for} \\ \quad i \in (-I_1, -I_0] \cup [I_0, I_1) \\ \qquad \vdots \\ \bar{d}_{ii} + \delta_{ii_{1_N}}|i| + ... + \delta_{ii_{4_N}}i^4, \text{ for} \\ \quad i \in \left(-I_N, -I_{N-1}\right] \cup \left[I_{N-1}, I_N\right) \end{cases},$$

$$\bar{d}_{ij} + d_{ij}(i,j) = \tag{15}$$

$$\begin{cases} \bar{d}_{ij}+\delta_{ij_{1_1}}|i||j|+\delta_{ij_{2_1}}i^2|j|+\delta_{ij_{3_1}}|i|j^2+ \\ +\delta_{ij_{4_1}}|i|j^3+\delta_{ij_{5_1}}i^3|j|+\delta_{ij_{6_1}}i^2j^2, \text{ for} \\ \quad i \in (-I_1,-I_0]\,\mathrm{U}\,[I_0,I_1) \\ \quad j \in (-J_1,-J_0]\,\mathrm{U}\,[J_0,J_1) \\ \qquad ... \\ \bar{d}_{ij}+\delta_{ij_{1_N}}|i||j|+\delta_{ij_{2_N}}i^2|j|+\delta_{ij_{3_N}}|i|j^2+ \\ +\delta_{ij_{4_N}}|i|j^3+\delta_{ij_{5_N}}i^3|j|+\delta_{ij_{6_N}}i^2j^2, \text{ for} \\ \quad i \in \left(-I_N,-I_{N-1}\right]\,\mathrm{U}\,\left[I_{N-1},I_N\right) \\ \quad j \in \left(-J_N,-J_{N-1}\right]\,\mathrm{U}\,\left[J_{N-1},J_N\right) \end{cases}$$

where $I_0 = J_0 = 0$. By this means, complex hydrodynamics characteristics may be estimated with high accuracy since hydrodynamic couplings among the modes are taken into account.

In order to involve only measurable signals in the estimation, high derivatives like $\dot{\mathbf{v}}$ are to be avoided. To this goal, the instrumental vector $\mathbf{z}$ is defined by filtering the acceleration $\dot{\mathbf{v}}$ such that

$$\mathbf{z} = \frac{1}{s+\lambda}\dot{\mathbf{v}} = \frac{s}{s+\lambda}\mathbf{v}, \tag{16}$$

where λ is a positive real-valued filter constant. So, with (16) and (1), it results

$$\begin{aligned} \mathbf{z} = & -\frac{1}{s+\lambda}\left(M^{-1}C(\mathbf{v})\mathbf{v}\right) - \\ & -\frac{1}{s+\lambda}\left(M^{-1}D(\mathbf{v})\mathbf{v}\right) + \\ & +M^{-1}\frac{1}{s+\lambda}\left(\mathbf{F}_c+\mathbf{F}_b+\boldsymbol{\tau}\right). \end{aligned} \tag{17}$$

For the identification process one can build up a linear regression for each mode $i \in \{u,v,w,p,q,r\}$ in the form

$$z_i = \frac{s}{s+\lambda}i = \boldsymbol{\phi}_i^T\boldsymbol{\theta}_i, \tag{18}$$

$$\begin{aligned} \boldsymbol{\phi}_i^T = \Bigg[& \frac{-1}{s+\lambda}u^2,\cdots,\frac{-1}{s+\lambda}ij,\cdots,\frac{-1}{s+\lambda}r^2, \\ & \frac{-1}{s+\lambda}u,\cdots,\frac{-1}{s+\lambda}r, \\ & \frac{-1}{s+\lambda}|u||i|i,\frac{-1}{s+\lambda}u^2|i|i,\cdots,\frac{-1}{s+\lambda}u^2i^3,\cdots, \\ & \frac{-1}{s+\lambda}|i|i,\cdots,\frac{-1}{s+\lambda}i^5,\cdots, \\ & \frac{-1}{s+\lambda}|r||i|i,\frac{-1}{s+\lambda}r^2|i|i,\cdots,\frac{-1}{s+\lambda}r^2i^3, \\ & \frac{1}{s+\lambda}\left(F_{c_u}+\tau_u\right),\cdots,\frac{1}{s+\lambda}\left(F_{c_r}+\tau_r\right)\Bigg] \end{aligned} \tag{19}$$

$$\begin{aligned} \boldsymbol{\theta}_i^T = \Big[& c_{i_1}^{'},\cdots,c_{i_k}^{'},\cdots,c_{i_{20}}^{'}, \\ & \bar{d}_{i_1}^{\prime},\cdots,\bar{d}_{i_6}^{\prime},\delta_{ui_1}^{'},\cdots,\delta_{ui_6}^{'},\cdots, \\ & \delta_{ii_1}^{\prime},\cdots,\delta_{ii_4}^{'},\cdots,\delta_{ri_1}^{'},\cdots,\delta_{ri_6}^{'}, \\ & m_{i_1}^{\prime},...,m_{i_6}^{\prime}\Big], \end{aligned} \tag{20}$$

where $c_{i_k}^{'}$ is one of the 20 constants contained in the row i of the matrix $M^{-1}C(\mathbf{v})$, $\bar{d}_{i_k}^{\prime}$ one of the 6 constants involved in the row i of $M^{-1}D_0$, $\delta_{ji_k}^{\prime}$ one of the 34 constants concerned in the row i of $M^{-1}D_1(\mathbf{v})$, and finally $m_{i_k}^{\prime}$ is the element k of the row i of M^{-1}. Furthermore, there exists one regressor z_i for each one of the N regions of the partition according to (14)-(15).

The dimension of the regressor vector $\boldsymbol{\phi}_i$ is 66 and can expand the whole space of parameters $\Re^{66}$ if certain conditions for the excitation $(\mathbf{F}_c+\mathbf{F}_b+\boldsymbol{\tau})$ are fulfilled as seen next.

4.1 *Identifiability*

The basis functions contained in the regressor (19) are linearly independent in $i,j \in \Re$, i.e., there exists no set of real constants $\{\alpha_1,...,\alpha_n\}$, with $1 < n \leq 66$, other than the trivial set $\{0,...,0\}$, that fulfills

$$\alpha_1\, g_1(i_1,j_1)+\cdots+\alpha_n\, g_n(i_n,j_n) = 0, \tag{21}$$

with $i_1,j_1,i_n,j_n \in \{u,v,w,p,q,r\}$. However, when a partition of the velocity space is considered according to (14)-(15), the linear independence of the basis functions is only ensured in the region about $\mathbf{v} = \mathbf{0}$, i.e., in $(-I_1,I_1)\times(-J_1,J_1)$. Outside this region, the set of functions $\left\{-\frac{1}{s+\lambda}i^2,-\frac{1}{s+\lambda}ij,-\frac{1}{s+\lambda}|i|i,-\frac{1}{s+\lambda}|i|j\right\}$ can only span a two-dimensional manifold of $\Re^4$. Consequently, parameters associated with the basis functions $-\frac{1}{s+\lambda}i^2$ and $-\frac{1}{s+\lambda}|i|i$ (or $-\frac{1}{s+\lambda}ij$ and $-\frac{1}{s+\lambda}|i|j$) are not distinguishable any more and identifiability gets lost.

To avoid this lack of identifiability one defines a second regression for each mode i in the form

$$\bar{z}_i = z_i - \sum_{\substack{k=1 \\ i,j\in\{u,v,w,p,q,r\}}}^{20} c_{i_k}^{'}ij, = \bar{\boldsymbol{\phi}}_i^T\bar{\boldsymbol{\theta}}_i, \tag{22}$$

$$\text{for } i\times j \notin (-I_1,I_1)\times(-J_1,J_1)$$

$$\bar{\boldsymbol{\phi}}_i^T = \left[-\frac{1}{s+\lambda}u,\cdots,\frac{1}{s+\lambda}\left(F_{c_r}+\tau_r\right)\right] \tag{23}$$

$$\bar{\boldsymbol{\theta}}_i^T = \left[\bar{d}_{i_1}^{\prime},\cdots,m_{i_6}^{\prime}\right] \tag{24}$$

where, in comparison with (18), only the terms up the position 21 are considered in the new regression. The regression is valid in all regions of the velocity space but not in the region that contains $\mathbf{v} = \mathbf{0}$. Thus the space of parameters is reduced to 46 dimensions.

4.2 *Algorithm*

For each regression z_i $(i = 1,...,6)$ and for each region of a partition according to (14)-(15), a lot of estimators in norm 2, such as of the type of the least-squares algorithm in continuous time, is applied in $i\times j \in (-I_1,I_1)\times(-J_1,J_1)$ (Ioannou and Sinn, 1995). Hence, the parameter adaptive law is

$$\hat{\dot{\boldsymbol{\theta}}}_i = P_i\varepsilon_i\boldsymbol{\phi}_i, \text{ con } \hat{\boldsymbol{\theta}}_i\,(0) = \begin{cases} \mathbf{0} \text{ for } t{=}0 \\ \hat{\boldsymbol{\theta}}_i\,(t_f) \end{cases} \tag{25}$$

$$\varepsilon_i = z_i - \hat{z}_i \tag{26}$$

$$\dot{P}_i = \beta P_i + P_i \boldsymbol{\phi}_i \boldsymbol{\phi}_i^T P_i,\ P_i(0) = \begin{cases} P_{0_i} \text{ for } t=0 \\ P_i(t_f) \end{cases} \tag{27}$$

$$\hat{z}_i = \boldsymbol{\phi}_i^T \hat{\boldsymbol{\theta}}_i, \tag{28}$$

where $\hat{\boldsymbol{\theta}}_i\ (t)$ is an estimate of (20) at t, $\hat{z}_i$ the estimation of the z_i with $\hat{\boldsymbol{\theta}}_i$, $\beta > 0$ is a scalar forgetting factor and finally $P_i > 0$ is the covariance matrix. Every time that the velocity trajectory $\mathbf{v}(t)$ enters into a new region of the partition, the initial condition $\hat{\boldsymbol{\theta}}_i\ (0)$ of the trajectory $\hat{\boldsymbol{\theta}}_i\ (t)$ is reset to the last value that it took the last time it left this region, said at $t = t_f$. At the same time, the initial condition of the covariance matrix is also reset to the old value. In this way, the estimates corresponding to a particular region are frozen till up the trajectory passes through this region again. So the estimates can approach piecewise to the true values of the non-linear characteristics.

Finally, the estimation algorithm captures the estimates of the non-linear damping in the partitioned domain of the approximation according to (14)-(15). To apply the algorithm (25)-(28) in the regions $i \times j \notin (-I_1, I_1) \times (-J_1, J_1)$, one replaces $\hat{\bar{z}}_i$, $\hat{\bar{\boldsymbol{\phi}}}_i$, $\hat{\bar{\boldsymbol{\theta}}}_i$ according to (22)-(24) instead of $\hat{z}_i$, $\boldsymbol{\phi}_i^T$, $\hat{\boldsymbol{\theta}}_i$, respectively. When (22) is used, one takes the c'_{i_k}'s from the last estimates in $\hat{\boldsymbol{\theta}}_i$ in order to apply (25)-(28) in the region about the null value of $\mathbf{v}$.

Once the 12 regressions z_i and $\bar{z}_i$ are built in the form indicated above, the matrices $\hat{M}^{-1}$, $(\hat{M^{-1}C}(\mathbf{v}))$, $(\hat{M^{-1}}D_0)$ and $(\hat{M^{-1}}D_1(\mathbf{v}))$ can be determined from the estimation procedure. Then the physical matrices of the hydrodynamics are calculated uniquely from the expressions

$$\hat{M}_a = (\hat{M^{-1}})^{-1} - M_{rov} \tag{29}$$

$$\hat{C}_a\ (\mathbf{v}) = (\hat{M^{-1}})^{-1} (\hat{M^{-1}C}(\mathbf{v})) - C_{rov}(\mathbf{v}) \tag{30}$$

$$\hat{D}_0 = (\hat{M^{-1}})^{-1} (\hat{M^{-1}}D_0) \tag{31}$$

$$\hat{D}_1\ (\mathbf{v}) = (\hat{M^{-1}})^{-1} (\hat{M^{-1}}D_1(\mathbf{v})). \tag{32}$$

4.3 *Convergence*

Proper excitation conditions are needed for achieving parameter convergence. One of these conditions involves the concept of persistency of excitation (PE) which stipulates that $\boldsymbol{\phi}_i(t)$ must satisfy in $t \in [t_0, t_1]$

$$\int_{t_0}^{t_1} \left(s^T \boldsymbol{\phi}_i(\tau)\right)^2 d\tau \geq \varepsilon_0, \tag{33}$$

where s is a any vector in $\Re^{66}$ (or $\Re^{46}$ for (22)) with Euclidean norm $|s| = 1$, and ε_0 is the so-called level of persistency.

One notices from (19) that for $\boldsymbol{\phi}_i$ to span the parameter space, there must exist motions in all modes. Other restrictions concern the force $(\mathbf{F}_c + \mathbf{F}_b + \boldsymbol{\tau})$, but specially $\boldsymbol{\tau}$ which is manipulated so that the vehicle can achieve a trajectory that makes each $\boldsymbol{\phi}_i$ to be PE.

The presence of a nonlinearity in the dynamics favors the search of a profile $\boldsymbol{\tau}(t)$ with sufficiently richness for accomplishing (33). One possibility is to use natural excitation produced on the vehicle and cable from normal manipulation of the ROV thrusters. Other possibility consists in generating a test signal for specially achieving the parameter estimation. This can be applied as much in test tanks as in natural environment with $\mathbf{F}_e = 0$. In particular, one can select uniformly bounded smooth signals

$$\tau_u(t) = a_u \sin(\omega_u t) \tag{34}$$

$$\cdots$$

$$\tau_r(t) = a_r \sin(\omega_r t), \tag{35}$$

with the condition that all ω_i and ω_j are pairwise different, and that together with the amplitudes a_i be large enough in magnitude to excite the vehicle in the prescribed velocity space covering all regions of the partition.

Using these components for $\boldsymbol{\tau}$, first 6 mutually linear independent basis functions $\{\frac{1}{s+\lambda}(F_{c_u} + \tau_u)$, $\ldots$, $\frac{1}{s+\lambda}(F_{c_r} + \tau_r)\}$ are generated in (19). This causes also other 6 mutually linearly independent set $\{\frac{-1}{s+\lambda}u, \ldots, \frac{-1}{s+\lambda}r\}$. Besides, $\frac{\mathbf{F}_c+\boldsymbol{\tau}}{s+\lambda}$ and $\frac{-\mathbf{v}}{s+\lambda}$ are also linear independent vector functions. The rest of the basis functions in (19), i.e., $\left\{\frac{-1}{s+\lambda}|j|^n|i|^m, \frac{-1}{s+\lambda}ij\right\}$ for $m, n \geq 1$, clearly results with the proposed excitation (34)-(35) in also linear independent basis functions.

In this way, the asymptotic convergence of the estimates using the algorithm (25)-(28) is ensured in each partition. It is worth noticing that certain parameters are instrumental in the sense that are estimated redundantly in different partitions, such as $\{m'_{i_1}, \ldots, m'_{i_6}\}$. In the limit for $t \to \infty$, these estimates will tend to the true values asymptotically.

Parallel to the excitation (34)-(35), which is synthesized, one can expect that perturbations of stochastic nature can reinforce the level of persistency and increment the rate of convergence. Also operation signals are rich enough in short periods, mainly by the regulation about a fixed point.

5. SIMULATIONS OF A CASE STUDY

Let us consider a vehicle with spherical form with $d = 1\,[\text{m}]$, a volume $V_{rov} = \frac{\pi D^3}{6} = 0{,}5236$

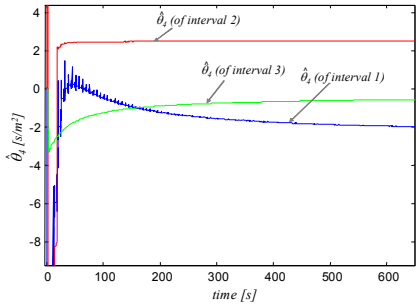

Fig. 4. Evolution of an estimate of the non-linear damping in different regions

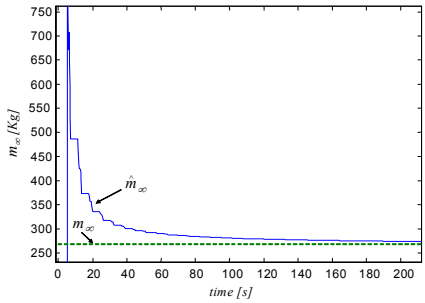

Fig. 5. Evolution of $\hat{m}_\infty$

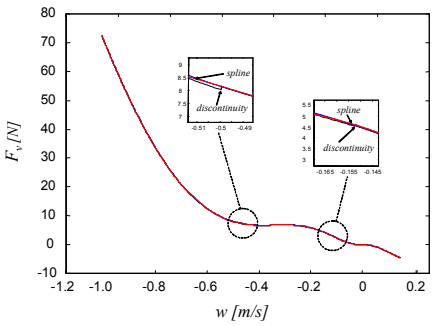

Fig. 6. Drag force characteristic in the mode w

[m^3], a transversal area $A_w = \frac{\pi\rho D^2}{4} = 0{,}7853$ [m^2] and a mass $m = 590.36$ [Kg]. Using existing radially symmetry in the distribution of mass and volume, the additive mass in the diagonal elements for the translations is $m_\infty = 268.35$ [Kg]. The couplings of the modes in the nonlinear damping are null and also null for every rotation mode.

So for this case study it is sufficient to excite the vehicle in only one mode to identify the whole hydrodynamics. The simulation results presented above correspond to the heave mode w. A partition of a velocity space $[-1.2\,[m/s], 1.2[m/s]]$ in $N = 3$ intervals, namely: $(-0.15, 0.15)$, $(-0.5, -0.15]$U$[0.15, 0.5)$ and $(-1.0, -0.5]$U$[0.5, 1.0)$, is sufficient in order to capture strong nonlinearities in the damping characteristic accurately (cf. drag force for $d = 1$ in Fig. (3), left). An external force with sinus form and $\omega = 1$ [rad/s] is applied to produce a vertical motion.

The coefficient λ for filtering the acceleration was set in $\lambda = 10$ [1/s] and $P_i(0)$ is selected diagonal with terms which are proportional to 10^n, where n is the order of the corresponding regressor element in (19). For instance, $P_i(0) = \alpha\,\mathrm{diag}(10^2, 10^2, ..., 1, 1)$, with $\alpha > 0$.

Fig. (4) shows the evolution of one parameter corresponding to the basis function $\frac{-1}{s+\lambda}|w|w^2$ in the different intervals. A relatively rapid convergence is achieved in the interval 2 located in the middle of the velocity space. In Fig. (5) it is seen the evolution of the added mass m_∞, which tends asymptotically to the true value. Finally, in Fig. (6) shows the piecewise reconstruction of the drag force characteristic in the velocity space with good coincidence with the true curve. At the connection points of the different paths it was applied a spline the order 3 for achieving continuity.

6. CONCLUSIONS

In this work an algorithm for on-line estimation of the hydrodynamics in underwater vehicles is presented. The identification comprehends matrices related to the added mass, the linear and non-linear drag, and the Coriolis and centripetal terms. It is required the measure of the thruster and cable forces and the velocity of the vehicle. Identifiability and convergence of the parameter trajectories are analyzed. The nonlinear drag is approximated by skew symmetric basis functions of the velocity components to a high degree of precision. A case study of a spherical ROV shows the features of the algorithm by numerical simulations.

7. REFERENCES

Beltrán-Aguedo, R. and Jordán, M.A., "A method for continuous-time identification of moored systems". Latin American Applied Research (LAAR), 33(4), 483-488, 2003.

Caccia, M. and Veruggio, G., "Guidance and control of a reconfigurable unmanned underwater vehicle". Control Engineering Practice 8, 21-37, 2000.

Do, K.D., Jiang, Z.P., Pan, J. and Nijmeijer, H., "A global output-feedback controller for stabilization and tracking of underactuated ODIN: A spherical underwater vehicle". Automatica, 40, 117 - 124, 2004.

Faltinsen, O.M., "Sea loads on ships and offshore structures". Cambridge University Press, 1993.

Fossen, T.I.,"Guidance and control of ocean vehicles". John Wiley & Sons Ltd., 1994.

Hideshi H., "Drag coefficient and upstream influence in three-dimensional stratified flow of finite depth". Fluid Dynamics Research, 4, 317-332, 1989.

Ioannou, P. A. and Sun, J., "Robust adaptive control". PTR Prentice-Hall, Upper Saddle River, 1996.

Kreuzer, E. and Pinto, F.C., "Controlling the position of a remotely operated underwater vehicle". Applied Math. and Comp., 78, 175-185, 1996.